IEEE Access
Multidisciplinary | Rapid Review | Open Access Journal

SPECIAL SECTION ON INTERNET OF THINGS (IoT) IN 5G WIRELESS COMMUNICATIONS

Received May 6, 2016, accepted May 30, 2016, date of publication June 24, 2016, date of current version July 21, 2016.

Digital Object Identifier 10.1109/ACCESS.2016.2584178

Enabling Massive IoT in 5G and Beyond Systems: PHY Radio Frame Design Considerations

AYESHA IJAZ, LEI ZHANG, MAXIME GRAU, ABDELRAHIM MOHAMED, SERDAR VURAL, ATTA U. QUDDUS, MUHAMMAD ALI IMRAN, CHUAN HENG FOH, AND RAHIM TAFAZOLLI

5G Innovation Centre, Institute for Communication System, University of Surrey, Guildford GU2 7XH, U.K.

Corresponding author: L. Zhang (lei.zhang@surrey.ac.uk)

This work was supported in part by the University of Surrey through the 5G Innovation Centre Programme, in part by the U.K. Engineering and Physical Science Research Council, and in part by NEC Telecom Modus Ltd., through the Industrial Cooperative Awards in Science and Technology Studentship.

ABSTRACT The parameters of physical layer radio frame for 5th generation (5G) mobile cellular systems are expected to be flexibly configured to cope with diverse requirements of different scenarios and services. This paper presents a frame structure and design, which is specifically targeting Internet of Things (IoT) provision in 5G wireless communication systems. We design a suitable radio numerology to support the typical characteristics, that is, massive connection density and small and bursty packet transmissions with the constraint of low-cost and low complexity operation of IoT devices. We also elaborate on the design of parameters for random access channel enabling massive connection requests by IoT devices to support the required connection density. The proposed design is validated by link level simulation results to show that the proposed numerology can cope with transceiver imperfections and channel impairments. Furthermore, the results are also presented to show the impact of different values of guard band on system performance using different subcarrier spacing sizes for data and random access channels, which show the effectiveness of the selected waveform and guard bandwidth. Finally, we present system-level simulation results that validate the proposed design under realistic cell deployments and inter-cell interference conditions.

INDEX TERMS 5G, frame structure, Internet of Things, random access channel.

I. INTRODUCTION

5th Generation (5G) wireless communication systems are expected to address unprecedented challenges to cope with a high degree of heterogeneity in terms of: (a) services (mobile broadband, massive machine and mission critical communications, broad-/multicast services and vehicular communications); (b) device classes (low-end sensors to high-end tablets); (c) deployment types (macro and small cells); (d) environments (low-density to ultra-dense urban); (e) mobility levels (static to high-speed transport) [1]. Therefore, 5G will provide an order of magnitude improvement in some key characteristics to efficiently support such heterogeneity with diverse set of requirements including, but not limited to, capacity/user-rates, latency, reliability, coverage, mobility, massive number of devices, cost/energy consumption. More specifically, 5G air-interface will achieve: (i) 1000× higher mobile data volume per geographical area; (ii) 10 to 100× more connected devices; (iii) 10 to 100× higher typical user data rate; (iv) 10x lower energy consumption; (v) sub-millisecond level end-to-end latency; (vi) ubiquitous 5G access including in low density areas [2].

The above mentioned fundamental characteristic are envisioned based on a number of emerging use cases and scenarios specified by the 5G research community [2]–[4]. For example, Mobile and Wireless Communications Enablers for the Twenty-Twenty Information Society (METIS) introduced 5 different scenarios and 12 test cases based on these scenarios [2]. Next Generation Mobile Networks (NGMN) has developed 25 use cases for 5G that are grouped into 8 use case families [4]. Ranging from high speed entertainment applications in a vehicle to smart meters installed in homes, from ultra-low latency vehicle-to-vehicle communication to delay-tolerant ubiquitous things communicating, and from ultra-reliable applications to best-effort services; different applications and uses cases can be categorized into four main communication scenarios [3]:

(i) Bitpipe communication: targets ultra-high user data rates and ultra-high traffic volume density in local indoor and outdoor hot-spot areas.

(ii) Internet of Things (IoT): this scenario targets sensory and data collecting use cases such as smart grid, health and environmental measurements, and monitoring etc.

(iii) Tactile Internet: this scenario focusses on special applications and use cases of IoT and vertical industries with real-time constraints such as Internet of Vehicles (IoV) and industrial control.

(iv) Wireless Regional Area Network (WRAN): this scenario focusses on coverage of low populated remote areas which suffer from low data rates and unreliable solutions.

To meet diverse requirements of 5G, an efficient, scalable and flexible air-interface is required and, therefore, different modules of both Physical (PHY) layer and Medium Access Control (MAC) layer should be optimized so that they can be configured flexibly according to the technical requirements of each scenario. However, PHY layer has a crucial impact on the efficiency and quality of the communication network as perceived by the users because: (i) it imposes limits to the basic parameters, for example the maximum data rates and granularity; (ii) the MAC efficiency rests on the capabilities and performance of the PHY layer [5].

A suitable frame structure is fundamental in the PHY layer design for achieving the challenging targets of 5G. Third Generation Partnership Project (3GPP) recently approved a study item on next generation new Radio Access technology (RAT) and work on frame structure was allocated high priority along with other areas of fundamental physical layer signal structure for new RAT [6]. Under the framework of METIS project, a Time Division Duplexing (TDD) frame structure was proposed and optimized for 5G air interface for mobile broadband in Local Area (LA) environment in [7] and [9]. Authors in [10] also derived a new flexible TDD-based radio interface parameterization for 5G LA communications combining the best practices of both WiFi and 3GPP Long Term Evolution-Advanced (LTE-A) technologies. Numerical analysis in [9] and [10] also showed reduced energy consumption of the network devices utilizing the respective proposed frame structures. A novel frame structure for ultra-dense 5G outdoor radio access networks was proposed in [11] and simulation results showed 2.4 times improvement in area spectral efficiency in low mobility scenarios compared to that of LTE. Radio numerology for 5G wide area system was designed in [12] to enable low latency with tolerable overhead while maintaining common clock with the LTE radio technology and robustness to hardware (HW) impairments. Authors in [13] have proposed a design for 5G frame structure for Frequency Division Duplex (FDD) cases applicable for macro-cell deployments in the framework of the Horizon 2020 project FANTASTIC-5G [1]. This solution encompasses flexible multiplexing of users on a shared channel with dynamic adjustment of the Transmission Time Interval (TTI) in coherence with service requirement per link. It defined a subcarrier spacing such that the smallest building block (a tile of time-frequency resources) can enable a very short (i.e. 0.2 ms) TTI to support sub-millisecond latency for delay sensitive applications.

It is observed from the literature [1], [7]–[13] that current frame designs for 5G networks are mainly focused on supporting 1 ms over the air communication latency. This is achieved by designing a numerology with large subcarrier spacing which leads to short symbol duration and, hence, short frame duration. The same subcarrier spacing is used for all the envisioned services and applications. However, over-the-air communication latency target of 1 ms has been set for ultra-low latency in tactile internet scenario only. Besides short radio frame, ultra-low latency also requires that tactile applications be kept local, close to the user [14]. Diverse performance requirements of different scenarios imply that different parameters of 5G frame structure should be flexibly configured to ensure an efficient usage of radio resources while coping with the design requirements of a mixture of services. Therefore, we need to design optimized radio numerology for each scenario. This can be done by taking into account different requirements and characteristics of each scenario and selecting the most suitable numerology to enable the best performance (in terms of Key Performance Indicators (KPIs)) for the corresponding scenario.

Since 5G is considered an important enabler for the IoT [15], we focus on the design of radio numerology for this scenario in this paper. IoT scenario is mainly characterized by small data packets, massive connections of devices with limited power source, and delay tolerant communication. Burst transmission of small data packets implies that such IoT devices do not need large channel bandwidth. In fact, narrow band system design can improve system coverage, power consumption, and reduce terminal cost [16]. Current frame structures with large subcarrier spacing are suitable for large bandwidth operation assumed in [7]–[13]. However, small bandwidth operation calls for adoption of small subcarrier spacing in IoT applications as will be discussed later in this paper.

In the IoT scenario, low-energy consumption devices are expected to be in Radio Resource Control (RRC) idle mode for most of the time [17]. Thus, scheduling requests may only be made using random access (RA) while in LTE/LTE-A they are usually handled by the Physical Uplink Control Channel (PUCCH) for the user equipments (UEs) in RRC connected mode [18], as explained in Appendix. Hence, a significant amount of research is being carried out to improve LTE's RA procedure for high traffic load [19]–[21]. To prevent high Machine-to-Machine (M2M) traffic load from adversely affecting Human-to-Human (H2H) traffic, Access Class Barring (ACB) [22] is a standardized approach in LTE/LTE-A. The core principle is to assign different Random Access Channel (RACH) access perseverance levels to different traffic classes in order to ensure that high priority users do not suffer from congestion caused by low priority ones. Dynamic RACH allocation [23] is another technique proposed to alleviate the high RACH load problem

in LTE/LTE-A, which is based on allocating additional RACH resources according to current traffic load conditions. However, while LTE/LTE-A is aimed at achieving a 99% RA success probability, it is commonly accepted that a higher collision probability is expected for the IoT scenario [21]. A tradeoff between tolerable access delay, limited control overhead, energy efficiency, and user density is therefore a major challenge for RA in M2M communications. In this paper, the proposed frame design provides sufficient RACH resources for IoT devices. The principle in doing so is to overprovision (i.e. provide more preambles than the expected maximum traffic so as to meet collision probability requirements) while keeping a reasonable control overhead and enabling a target of high user density.

It must be noted that the waveform modulation scheme adopted at the PHY layer will not only impact all the requirements and advanced technologies of 5G cellular systems, it will also impact the radio numerology design. Orthogonal Frequency-Division Multiplexing (OFDM) has been adopted as the air interface in several wireless communication standards, including LTE and IEEE 802.11 standard families due to the associated advantages such as robustness against multi-path fading, ease of implementation, efficient one-tap frequency domain equalization enabled by the use of Cyclic Prefix (CP), straightforward and simple extension to very large Multiple Input Multiple Output (MIMO), and high gain beamforming solutions. However, OFDM also suffers from a number of drawbacks including high Peak-to-Average Power Ratio (PAPR) and poor spectral containment. It shows increasing signaling overhead with the number of UEs due to stringent time synchronization required to maintain the orthogonality between different UEs. Moreover, it has high sensitivity to Carrier Frequency Offset (CFO) mismatch between different devices. All these drawbacks hinder the adoption of OFDM in the 5G air interface. While different candidate waveforms are being investigated for 5G networks [24]–[27], to address the drawbacks of OFDM and achieve 5G requirements, Universal Filtered Multicarrier (UFMC) [3], [28]–[31] is considered as one of the strongest candidates due to its high degree of flexibility. UFMC system is also shown to be more robust to transceiver imperfections such as CFO and Timing Offset (TO) in [32] and [33] which is important for low-cost low-complexity IoT devices. Therefore, as an example, we adopt UFMC as a suitable waveform to show the frame design principles. However, the proposed framework and radio design can also be adopted for other waveforms albeit with minor modifications.

The main contributions of this paper are as follows:

- We elaborate on fundamental constraints for different frame design parameters. Based on these constraints, we provide some useful guidelines to select suitable numerology for frame design using UFMC waveform for air interface.
- We identify main requirements and deployment scenarios for sensory and data collection services in IoT scenario. Based on the derived guidelines for frame design, we determine suitable values of some fundamental parameters. We provide numerical results to describe the impact of different frame structure parameters on service requirements and propose an optimal numerology for low bandwidth operation to support massive connection density that is the most important requirement for the aforementioned services. We provide link level simulation results to verify that the proposed numerology can effectively cope with different transceiver imperfections and channel impairments. Simulation results also show that UFMC based system has improved performance as compared to an OFDM based system. System level simulation results are also presented to show the connection density achieved with the proposed frame design under realistic cell deployment configurations and inter-cell interference conditions.
- Apart from suitable numerology to support data communication from massive number of connections, PHY layer frame should also cope with the resources required to handle the corresponding massive connection establishment and scheduling requests. Hence, we also elaborate on design of parameters for RACH in this paper. Use of different subcarrier spacing for different channels (e.g. data and RACH) in adjacent bands results in interference between the bands. Therefore, Guard Band (GB) between the bands must be carefully selected. Simulation results are provided in this paper to show that UFMC can outperform OFDM in this situation. Moreover, simulation results also indicate that the selected value of GB for frame design can cope with the interference and avoid performance degradation.
- The PHY layer design of 5G cellular systems is currently actively being discussed in various industrial fora, standardization bodies such as 3GPP [6], and academic circles. This paper aims to contribute towards this discussion and highlights the trade-offs that must be made in order to reach expected performance targets and the constraints imposed by radio channels, device technology, and the offered flexibility of the system.

The rest of the paper is organized as follows. Section II provides some useful guidelines to elaborate on the principles of radio numerology design. Based on these principles, proposed frame design for IoT is described in Section III. Section IV presents link level simulation results to show the performance of the designed radio numerology in the presence of transceiver imperfections and comparison of UFMC based system with an OFDM based system. System level simulation results are also given in Section IV to assess the system performance and capacity in realistic conditions. Finally, concluding remarks are given in Section V.

II. GUIDELINES FOR FRAME DESIGN

In this section, we aim to provide some guidelines to follow for radio numerology design. We focus on frame design for dynamic TDD deployment [34] since it is considered

more attractive than FDD to match the diverse quality of service requirements imposed by a variety of 5G applications. TDD also offers the possibility to exploit channel reciprocity avoiding feedback overhead particularly in massive MIMO. Moreover, results in [34]–[39] have shown that dynamic TDD provides substantial system performance improvement as compared to static TDD.

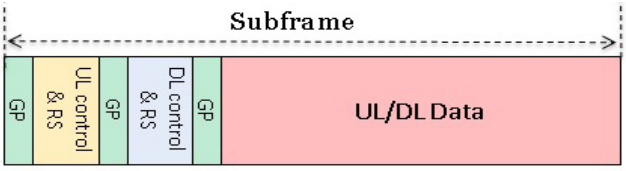

FIGURE 1. TDD Subframe Structure.

For radio frame numerology design we assume the subframe structure given in [7] as shown in Fig. 1 wherein Uplink (UL) and Downlink (DL) control symbols and Reference Signals (RS) are embedded at the beginning of each subframe. Interested readers can refer to [40] for details on design of reference symbols pattern for 5G multicarrier modulations. The data symbols within each subframe can be dynamically scheduled to carry either UL or DL data depending on the user and/or service requirements. A Guard Period (GP) is inserted between UL and DL control symbols and between control and data region for each potential UL-DL and DL-UL transmission direction transition and to avoid transmitter power leakage in the receiver chain. UL and DL control region is assumed to carry Hybrid Automatic Repeat Request (HARQ) signaling [8] and scheduling related control information, such as scheduling requests and grants.

TABLE 1. Main parameters for radio numerology design.

Parameter	Description
B_s	Service bandwidth
B_G	Guard band
Δf	Subcarrier spacing
T_u	Useful symbol duration $(1/\Delta f)$
N_{FFT}	Fast Fourier Transform (FFT) size
f_s	Sampling frequency
T_s	Sampling interval $(1/f_s)$
N_{data}	Number of data symbols in subframe
N_{ctrl}	Number of symbols in UL/DL control region
L_{filter}	Subband filter length in samples
L_{ZP}	Zero prefix length in samples
T_{GP}	Guard period

Table 1 shows the main parameters for radio numerology design. In order to select suitable values of these parameters, we need to consider the interdependency of different parameters, service requirements, system, and channel characteristics as shown in Fig. 2. The parameters in pink shaded blocks indicate required input for frame design.

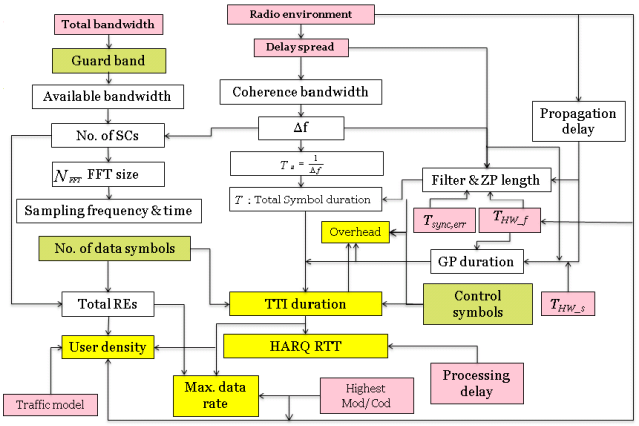

FIGURE 2. Interdependency of different subframe parameters and service requirements.

Whereas, green shaded blocks highlight parameters which must be determined analyzing their effect on different KPIs given in yellow blocks. The rest of the blocks contain parameters which can be either determined based on input parameters in conjunction with other parameters or which must adhere to certain constraints of system design as will be discussed later in this section.

We can see that the most important parameter in subframe design is subcarrier spacing Δf since most of the other parameters depend on this value either directly or indirectly. The value of Δf needs to be carefully chosen considering the propagation characteristics of the environment where the system is intended to operate. It also affects different service requirements such as user density, maximum data rate, subframe duration, and HARQ Round Trip Time (RTT). Other frame design parameters which depend on channel characteristics and impact service requirements include filter and GP lengths. We describe the above three parameters in more detail below.

A. SUBCARRIER SPACING

It can be seen from Fig. 2 that the subcarrier spacing directly affects the number of subcarriers (SCs), i.e. N_{SC}, for a fixed system bandwidth and, hence, total number of resource elements since each resource element corresponds to a subcarrier symbol. Therefore, it affects the FFT size as well as the maximum data rate. Subcarrier spacing also determines the useful symbol duration (T_u) since $T_u = 1/\Delta f$. Hence, it affects the subframe duration and, hence, HARQ RTT in addition to user density and PHY layer overhead.

Large subcarrier spacing means small symbol duration and vice versa. Therefore, large subcarrier spacing seems more suitable for latency critical applications such as tactile internet and Vehicle to Vehicle (V2V) communications. However, feasible subcarrier spacing range in the radio frame design is seriously constrained by the channel dispersions in both time and frequency domain. Specifically, subcarrier spacing must be within the channel coherence bandwidth in order to enable one tap frequency domain equalization. Therefore, following

constraint needs to be taken into account when determining maximum subcarrier spacing:

$$\Delta f_{max} \leqslant B_{C,90\%} \tag{1}$$

where $B_{C,90\%}$ is 90% channel coherence bandwidth which depends on Root Mean Square (RMS) delay spread of the channel (T_d) since $B_{C,900\%} = 1/50T_d$.

On the other hand, small subcarrier spacing makes the system more sensitive to Doppler spread. Generally, following constraint needs to be satisfied to keep Inter Carrier Interference (ICI) due to the Doppler spread sufficiently low:

$$\frac{f_{d_{max}}}{\Delta f} \ll 1 \tag{2}$$

where $f_{d_{max}}$ is the maximum Doppler spread. Small subcarrier frequency results in longer symbol duration and lower overhead, as will be explained in next section. Therefore, delay tolerant services can benefit from small subcarrier spacing to reduce overhead. However, it also makes the system more sensitive to Carrier Frequency Offset (CFO) and, therefore, the chosen value must be able to cope with transceiver imperfections.

It is evident from the above discussion that the characteristics of the radio channel must be known in addition to latency requirement of the communication scenario to select an appropriate value of subcarrier spacing when designing radio numerology for any scenario.

B. FILTER AND ZERO PREFIX LENGTH

Compared to OFDM, UFMC does not use CP and its additional symbol duration overhead is used to introduce sub-band filters [3]. The sub-band filters reduce Out of Band Emission (OBE) while the Zero Postfix/Prefix (ZP) accommodates the transient response of the sub-band filter, thereby, providing soft protection against Inter Symbol Interference (ISI) caused by delay spread.

To provide protection against ISI, intuitively, duration of filter tail, i.e. T_{filter}, must be within the duration of ZP (T_{ZP}) which, in turn, depends on the channel RMS delay spread as given below:

$$T_{ZP} \geq T_d \tag{3}$$

Actual ZP must also compensate for the transmitter and receiver hardware filter response to radio channel delay spread, i.e. T_{HW_f}, and ensure a safe margin to compensate for timing synchronization error (T_{sync_err}) between cells. Therefore, ZP duration is determined similar to CP length determination given in [7] as:

$$T_{ZP} = T_d + T_{HW\_f} + T_{sync\_err} \tag{4}$$

Note that in LTE/LTE-A, the channel propagation delay (T_{CH_prop}) is compensated by using a timing advance technique at the UE, which requires a further hand-shaking procedure before UL transmission can take place [41]. However, emergence of small-cell infrastructure in 5G networks [42] implies lower expected propagation delay. Therefore, signaling hand-shaking and additional latency in UL due to timing advance can be avoided by embedding the two way maximum channel propagation delay into the ZP as done for CP in [7]. Hence, ZP in small cells is determined as:

$$T_{ZP} = T_d + T_{HW\_f} + T_{sync\_err} + 2T_{CH\_prop} \tag{5}$$

The ZP length (in samples) can be determined from (4) or (5) as $L_{ZP} = T_{ZP,min}f_s$ where f_s is the sampling frequency determined as $f_s = N_{FFT} \cdot \Delta f$. Filter length based on delay spread, $L_{filter,DS}$, can now be calculated as:

$$L_{filter,DS} = L_{ZP} + 1 \tag{6}$$

In addition to mitigate ISI/ICI caused in multi-path fading channel, one should note that one of the primary objectives for using sub-band filters in UFMC is to reduce OBE to minimize the adjacent channel interference. A longer filter not only leads to a lower OBE, but also makes the system more robust to errors and multipath fading channel. However, a longer filter also causes several drawbacks including more frequency selective filter response along subcarriers within one sub-band and larger overhead. The analytical framework, provided by the authors in [43], for optimal filter length selection indicates that a reasonable filter length to minimize OBE, i.e. $L_{filter,OBE}$, while maximizing the system capacity is in the range from L_1 to $2L_1$ where $L_1 = \left\lceil \frac{N_{FFT}}{N_{SB}} \right\rceil$ and N_{SB} is the sub-band size (in terms of number of subcarriers). Therefore, we propose to determine the filter length and ZP as follows:

$$L_{filter} = L_{filter,OBE} = L_1 \text{to} 2L_1 \tag{7}$$

$$L_{ZP} = max\left(L_{filter,DS} - 1, L_{filter,OBE} - 1\right) \tag{8}$$

It can be noted from above discussion that cell size also needs to be known in addition to channel characteristics, hardware filter response to channel delay, and synchronization error between cells for filter and ZP length determination in frame design.

C. GUARD PERIOD LENGTH

A GP is used to control switching between transmission directions in the TDD mode. In a TDD device, the ramp-on and ramp-off delays of the power amplifier may create interference from transmitter to the receiver. Therefore, the GP must compensate the hardware switching time, T_{HW_s}. This is the time needed by the device to switch to/from 90% from/to 10% nominal power, and also include the gate lag time, needed to switch from the last 10% nominal power to adequate near-zero level [44]. The GP must also compensate for the channel propagation delay and the RMS delay spread towards the receiving devices before they switch to transmission mode. The filter response time to delay spread in transmitter and receiver, T_{HW_f}, also needs to be compensated by GP. Hence, the GP duration can be determined as given in [7] i.e.

$$T_{GP} = T_{HW\_f} + T_{HW_s} + T_{CH\_prop} + T_d \tag{9}$$

The GP is inserted at three potential UL-DL and DL-UL transmission directions in the proposed subframe as shown in Fig. 1. Hence, it can contribute significantly towards PHY layer overhead. Therefore, the values of different components in (9) must be carefully evaluated taking into account the radio channel environment, and the component technology enhancements.

III. FRAME DESIGN FOR IoT

In this section, we propose frame design for IoT focusing on delay tolerant, low-power and massive connection scenario. Before we can design radio numerology for this scenario, its service requirements and the radio channel characteristics must be defined. The proposed frame design must meet service requirements as closely as possible while satisfying different design constraints as mentioned in the previous section.

TABLE 2. KPIs for massive, low-cost IoT communication scenario.

	KPI	Requirement
User experience requirements [4]	User experienced data rate	Low (typically 1-100 kb/s)
	End-to-End (E2E) latency	Seconds to hours
	Mobility	Low (0-3 km/h)
System performance requirements	Connection density	200,000/km^2 [4] 300,000 per cell [46] 1 million/km^2 [17]
	Coverage	99.9% [46]
	Protocol scalability	80% protocol efficiency at 300,000 devices per access node [46]
	Energy efficiency	0.015 uJ/bit for data rate in the order of 1 kb/s [46]

A. REQUIREMENTS AND CHARACTERISTICS

The user experience and system performance requirements for the IoT communications scenario under consideration are summarized in Table 2. The details of these KPIs can be found in [4] and [45]. Here, KPIs which are considered important from PHY layer frame design point of view include user experienced data rate, End-to-End (E2E) latency, mobility, and connection density. E2E latency accounts for the time needed for the data packet to cross all the nodes up to the application server and back, which includes nodes of the 5G system and nodes potentially outside the 5G system [4]. Therefore, E2E latency must be evaluated considering network topology, component technology enhancements, and higher layer processing delays. However, we focus on HARQ RTT, i.e. equivalent to four subframes duration [7], in this paper for radio numerology design. The most important KPI in this scenario is connection density and the target value is extremely high as can be seen from Table 2. Therefore, our objective in the following sections is to propose a radio design numerology which can achieve extremely high connection density for low data rate and delay-tolerant devices. We observe from the literature [4], [16], [45] that the target connection density value is different for different research groups. The UL capacity for low data rate Machine Type Communication (MTC) services was analyzed in [46] assuming the traffic model is that of a home monitoring service. The set up assumes an FDD system with 1.4 MHz bandwidth and two uncorrelated receive antennas at the Evolved Node-B (eNB). It was shown in [46] that LTE/LTE-A can support 48,000 device/MHz/cell using 16-QAM modulation in an urban macro-cell wherein Inter Site Distance (ISD) is 500 m. We set our connection density target to be at least 10 times higher which translates to required connection density of 480,000 device/cell.

User or connection density is defined as the number of devices that can be supported based on the required data rate within the cell [46]. Hence, as it can also be seen from Fig. 2, that the user or connection density depends on traffic model besides some other parameters, e.g., modulation scheme, code rate etc. We assume a payload of 125 bytes is transmitted with an average period of 5 minutes i.e. the non-real time application-driven traffic model for Massive Machine Communication (MMC) given in [47]. Therefore, for the scenario under consideration, traffic model parameters are summarized in Table 3.

TABLE 3. Traffic model for massive, low-cost IoT communication scenario.

Parameter	Value
S = Burst size [bytes] [48]	125
R = Inter packet delay [s] [48]	300
Average data rate [b/s] [48]	3.33
K = No. of users [per cell]	480,000
V = Traffic volume = K.S/R [Mb/s]	1.6

As explained in the previous section, we need to define radio channel characteristics for the environment where the system is intended to operate before we can design numerology for IoT frame in 5G. The assumed channel model parameters are given in Table 4. We assume two different deployment scenarios for IoT communications: i) Small cell scenario with cell size 0.1 km, and ii) Large cell scenario assuming cell size 10 km. It is anticipated that the channel models for evaluation of 5G systems will be available by the mid-2016 time frame [48]. Therefore, we assume currently used and widely recognized IMT-Advanced fading channel models [49] recommended by International Telecommunication Union (ITU) which can be parameterized for to up to 100 MHz bandwidth. The details of assumed channel models for two deployment scenarios can be found in [50]. We assume relatively higher carrier frequency (f_c) for small cell deployment as compared to the large cell deployment scenario due to relatively lower path loss in small cells. Assuming maximum velocity 3 km/h in both scenarios, maximum

TABLE 4. Channel characteristics for massive, low-cost IoT communication scenario.

Parameter	Value	
Cell size [km]	0.1 (small cell)	10 (large cell)
Channel model	ITU-R Umi NLoS	ITU-R UMa NLoS
Delay spread [ns]	129	365
$B_{C,90\%}$[kHz]	155.04	54.79
Carrier frequency [GHz]	3.5	1
Velocity [km/h]	3	3
$f_{d_{max}}$ [Hz]	9.728	2.78
Coherence time [ms]	51.4	180

Doppler spread is 9.728 Hz and 2.78 Hz in small and large cell, respectively. It can be seen that the channel coherence time is quite large in both deployment scenarios indicating that the channel varies very slowly over time due to low mobility.

B. NUMEROLOGY DESIGN

In this section, we design radio numerology for low-power, massive connection IoT communication scenario based on the design guidelines provided in Section II in two different deployment scenarios described in Section III.A.

As shown in Fig. 2, the most important frame design parameter is subcarrier spacing. According to (1), the maximum subcarrier spacing can be 155 kHz and 54 kHz in small and large cell deployment, respectively. However, it must be noted that IoT services featured with burst transmission of small data packets do not require large channel bandwidth. In fact, narrow band system design can improve system coverage, power consumption, and reduce terminal cost. Therefore, small subcarrier spacing seems more suitable to increase the pilot density and support narrow band system design for IoT. However, when the subcarrier spacing is very small, the receiver synchronization components need to be very accurate, which is not possible with low-cost Radio Frequency (RF) hardware. Hence, we assume minimum subcarrier spacing of 2 kHz that is nearly the same value as the minimum subcarrier spacing, i.e. 2.5 kHz for Narrow Band OFDMA (NB-OFDMA) [51], specified for different candidate clean slate solutions for massive connectivity in IoT scenario [51].

In order to find suitable value of Δf and other frame design parameters that can maximize the connection density, we analyze the impact of Δf and number of data symbols in a subframe on different user and system performance requirements. The preliminary frame design parameters are given in Table 5. We assume 200 kHz bandwidth that is inline with the envisaged narrow band IoT design [51]. Since, UFMC has improved spectral containment than OFDM [25], [26], guard band of 5% is assumed resulting in 190 kHz bandwidth available for transmission. Initially we assume the sub-band size $N_{SB} = 12$ subcarriers i.e. equivalent to the

TABLE 5. System and preliminary frame design parameters.

Parameter	Value
Bandwidth [kHz]	200
Guard band	5%
Available bandwidth [kHz]	190
N_{SB} [subcarriers]	12
T_{ZP} [μs] (from (5))	1.35 (small cell), 0.915 (large cell)
T_{GP} [μs]	0.57 (small cell), 33.8 (large cell)
UL/DL control symbols	1

Resource Block (RB) size in LTE/LTE-A. This value will be fine tuned depending on the final value selected for Δf. Using (4), (5), and (9), T_{ZP} and T_{GP} are calculated assuming different component delays and synchronization errors as given in [7] and [44].

Assuming there is only one UL and one DL control symbol (N_{ctrl_s}) in a subframe, subframe duration for the large cell deployment is shown in Fig. 3. This figure shows the subframe duration assuming value of Δf ranges from 1 kHz to 20 kHz while number of data symbols (N_{data}) in the subframe varies from 1 to 30. The subframe duration is determined as follows:

$$T_{subframe} = \left(2N_{ctrl\_s} + N_{data}\right)\left(T_u + T_{ZP}\right) + 3T_{GP} \qquad (10)$$

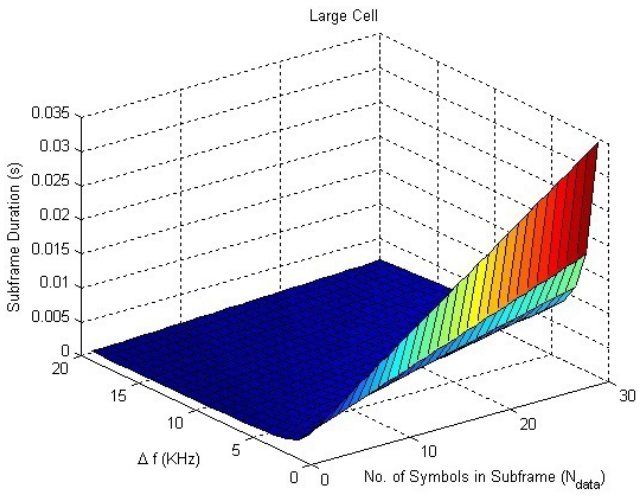

FIGURE 3. Subframe duration versus subcarrier spacing and data symbols.

Fig. 3 shows that subframe duration increases linearly with increase in N_{data}. However, the increase in $T_{subframe}$ is more noticeable at lower values of Δf due to relatively large symbol duration. It is also observed from this figure that the increase in T_u at lower values of Δf increases subframe duration for a fixed value of N_{data} in the subframe. Similar observations are made for HARQ RTT shown in Fig. 4. These results confirm that small subcarrier spacing

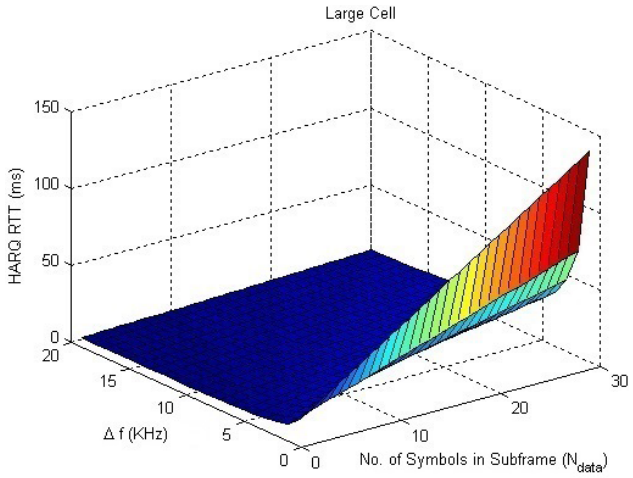

FIGURE 4. HARQ RTT versus subcarrier spacing and data symbols.

is only suitable for delay tolerant services. Since we focus on delay tolerant services, therefore, HARQ RTT is not a critical factor to influence the selection of radio numerology. Hence, we now analyze the impact of Δf and N_{data} on the total overhead (OH_{total}) determined as follows:

$$OH_{total} = OH_{ZP} + OH_{ctrl} + OH_{GP} \tag{11}$$

where ZP OH, control OH, and GP OH are defined as follows:

$$OH_{ZP} = \frac{\left(N_{data} + 2N_{ctrl\_s}\right) T_{ZP}}{T_{subframe}} \times 100 \tag{12}$$

$$OH_{ctrl} = \frac{\left(2.N_{ctrl\_s}\right) T_u}{T_{subframe}} \times 100 \tag{13}$$

$$OH_{GP} = \frac{3T_{GP}}{T_{subframe}} \times 100 \tag{14}$$

It must be noted that control overhead includes overhead due to control as well RS since RS are embedded within the control region.

Fig. 5 shows total overhead in small and large cell deployment versus subcarrier spacing and number of data symbols in a subframe. It can be seen from these results that total overhead decreases significantly with increase in number of data symbols in a subframe. This is due to the increase in subframe duration which results in relatively lower GP, control and ZP overheads. For a very large number of data symbols, total overhead is limited by the ZP overhead. The numerical results in Fig. 5 imply that moderate to higher number of data symbols must be selected for frame design to avoid large overhead for delay tolerant services.

It is observed from Fig. 5 that the total overhead is almost invariant to change in Δf for small cell deployment. However, in large cell deployment, the overhead increases with increase in subcarrier frequency. This can be explained by analyzing the impact of Δf on individual component overheads in (11) for a fixed value of N_{data} as shown in Fig. 6 and Fig. 7 for small and large cell, respectively, for $N_{data} = 12$. Since a large GP is required in large cell, to compensate for large propagation delay, GP overhead shows considerable increase with increase in subcarrier spacing in large cell deployment as compared to small cell scenario. Due to small bandwidth operation, sampling frequency is very small and, hence, $L_{ZP} = L_{filter,OBE} - 1$ that is proportional to $\left\lceil \frac{N_{FFT}}{N_{SB}} \right\rceil$. Since absolute value of T_{GP} is very small in small cell, this implies that $T_{subframe}$ decreases by almost the same proportion as reduction in filter length with increase in Δf. Hence, ZP overhead is almost invariant to the change in Δf in small cell.

However, in large cell deployment, there is slight reduction in ZP overhead at large subcarrier spacing due to large GP and, hence, increased subframe duration. Similarly, control overhead is also constant for a fixed number of data symbols in the subframe in small cell and shows slight reduction in large cell scenario at higher subcarrier spacing. Therefore, due to large GP in large cell deployment, total overhead shows

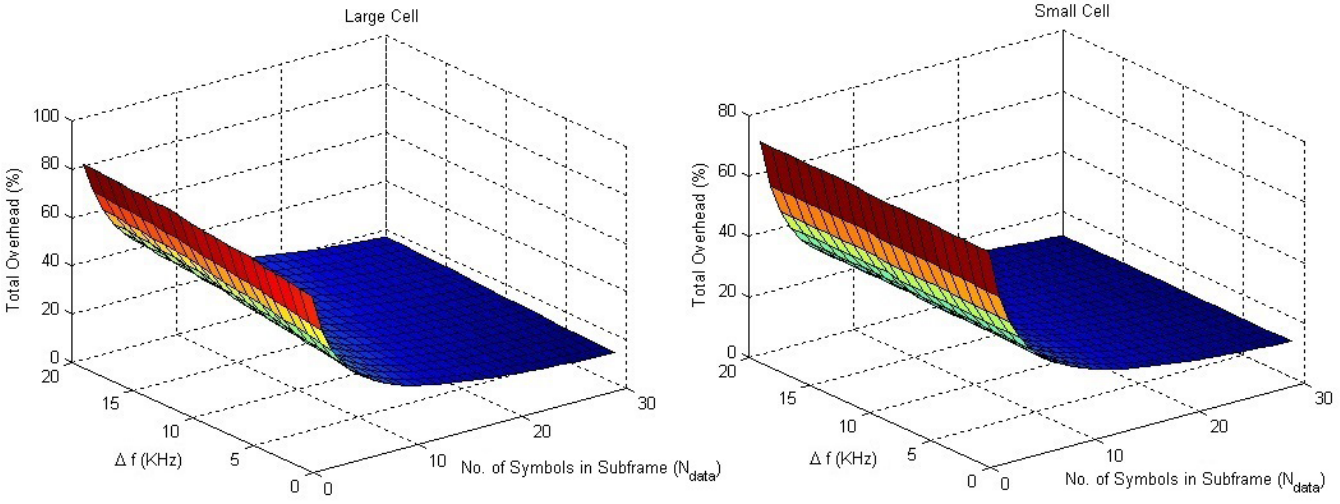

FIGURE 5. Total overhead versus subcarrier spacing and data symbols.

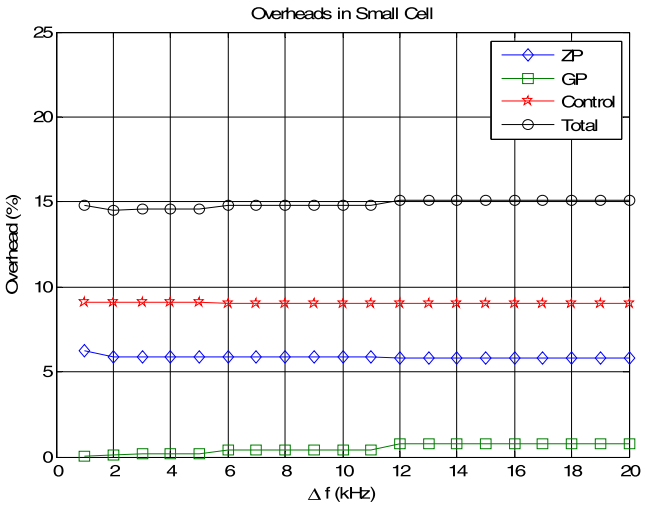

FIGURE 6. Overheads in small cell versus subcarrier spacing.

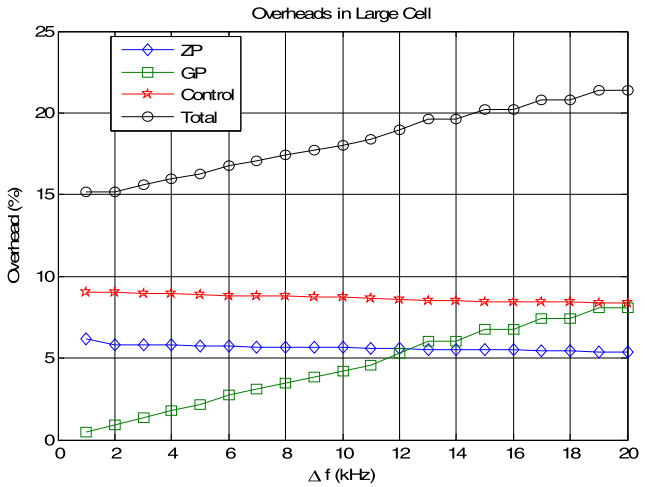

FIGURE 7. Overheads in large cell versus subcarrier spacing.

noticeable increase with increase in subcarrier spacing. However, small GP in small cell implies that total overhead shows negligible increase at higher values of subcarrier spacing.

It can be concluded from the numerical results that although small Δf increases subframe duration and, hence, HARQ RTT, it is more suitable to select small value of Δf to reduce PHY layer overheads particularly in delay tolerant communication scenario.

Now we observe the impact of change in Δf and N_{data} on the most important KPI for IoT, i.e. user density, assuming Quadrature Phase Shift Keying (QPSK) modulation without any error correction coding in two different deployment scenarios. Fig. 8 shows the resulting user density (users/km^2) that is number of users which can be scheduled within 300 s in an area of 1 km^2 assuming each user is transmitting 125 bytes in 300 s. It is assumed that minimum scheduling granularity is one sub-band and one user is scheduled to transmit only in one sub-band in one subframe. Therefore, minimum number of subframes (N_{fu}) required by a user to transmit a burst of S bytes using M bits per Quadrature Amplitude Modulation (QAM) symbol and code rate r is given as:

$$N_{fu} = \left\lceil \frac{S \times 8}{N_{SB} \times N_{data} \times M \times r} \right\rceil \tag{15}$$

Hence, the user density is determined as follows:

$$UserDensiy = \left\lfloor \frac{N_{SC}}{N_{SB}} \right\rfloor \times \left\lfloor \frac{R}{N_{fu} \times T_{subframe}} \right\rfloor \times \frac{1}{Cell\ Area} \tag{16}$$

While system level simulations are required to obtain more realistic values of supported user density, numerical results are also important for frame design. It is seen from Fig. 8 that overall user density increases with increase in N_{data} due to reduced overhead. However, for a fixed value of Δf, some fluctuations in user density are observed with change in N_{data}. This is due to variation in difference between the total number of available resource elements and the actual number of resource elements required to transmit a burst of 125 bytes.

Although, subframe duration decreases with increase in Δf as seen in Fig. 3, total number of resource elements within a given time interval remain almost constant due to corresponding decrease in number of subcarriers within one symbol duration. Hence, one would expect the user density to remain constant with change in Δf. However, we observe that the user density fluctuates and first decreases with increase in Δf before it starts increasing again. This is an artefact of the following assumption about minimum scheduling granularity in simulation settings. As mentioned earlier, minimum scheduling granularity is one sub-band, i.e. 12 subcarriers, unless the total number of available subcarriers is less than 12. In the latter case, one sub-band is assumed to contain total number of available subcarriers. Therefore, bandwidth efficiency (i.e. ratio of used subcarriers (N_{used}) and total available subcarriers (N_{SC})) varies with Δf causing variations in user density.

Based on the observations made in this section, we can conclude that small Δf and moderate number of data symbols seem suitable for IoT scenario to achieve a trade-off between user/connection density and PHY layer overhead. While a large number of data symbols reduces overhead and improves user density, a very large subframe duration is not preferred due to scheduling issues which may arise when different services with heterogeneous requirements are multiplexed in a 5G network. Therefore, we propose the numerology given in Table 6 for IoT frame in 5G along with the numerical values of different KPIs. Filter and guard period lengths are adjusted such that total number of samples in the subframe are equal in both deployment scenarios. It must be noted that this numerology is proposed for 200 kHz bandwidth operation only. When B_S changes, resulting number of subcarriers i.e. N_{SC} may not be exactly divisible by the proposed sub-band size i.e. $N_{SB} = 19$. Hence, N_{SB} will have to be defined according to the available number of subcarriers.

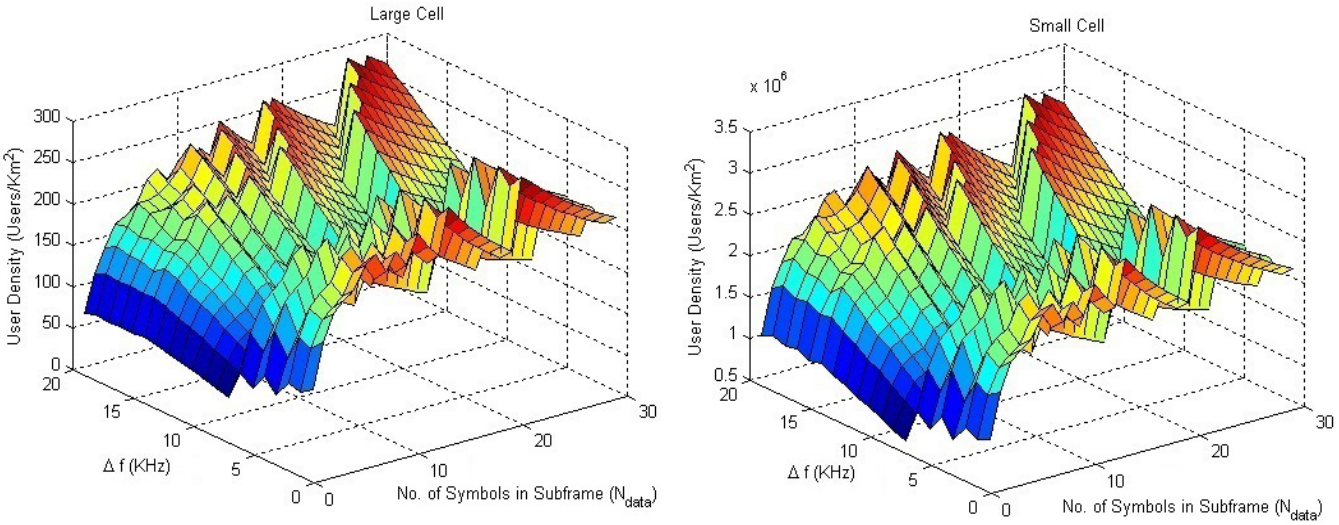

FIGURE 8. User density versus subcarrier spacing and data symbols.

As discussed in Section III, required connection density is 480,000 devices/cell which translates to 15.3M devices/km^2 and 1530 devices/km^2 in small and large cell, respectively. However, theoretically achievable connection density is 7.2 times lower than the target density. Therefore, in order to support 480,000 narrow band (i.e. 200 kHz) IoT devices in a cell, minimum eight 200 kHz fragments must be used by the base station wherein each device will still operate on 200 kHz fragment.

C. RANDOM ACCESS CHANNEL

As mentioned earlier in Section III.B, eight 200 kHz fragments need to be simultaneously allocated to achieve the target density of 480,000 users/cell. This, however, does not take into account specific control resources required to access the network and to request an initial grant, i.e. the RA procedure. Therefore, it is important to determine an appropriate number of available preambles and the frequency of RA slots in order to enable potentially large number of RA attempts to support massive connection density. In this section, we present a design that accommodates the high user density scenarios and narrow band operation.

In the proposed design, we consider that the radio frame consists of successive 200 kHz bands, for data and control, which are contiguous in frequency. However, it must be noted that non-contiguous and fragmented bands may also be used for data transmission.

The proposed design is preamble-based and builds on the LTE/LTE-A RA procedure, which is detailed in Appendix. The preamble sequence length is 864 symbols, as defined in LTE/LTE-A, and the subcarrier spacing is 231 Hz. This results in a 4.52 ms long preamble, including a 0.1 ms CP and a 0.1 ms Guard Time (GT), which are necessary to mitigate multipath fading and to tackle the propagation delay uncertainty, respectively. In this design, similarly to ACB,

TABLE 6. Proposed frame design parameters for IoT in 5G.

Parameter	Value	
B_s [kHz]	200	
Δf[kHz]	2	
T_u [ms]	0.5	
B_G[%]	5	
N_{SC}	95	
N_{FFT}	128	
f_s [kHz]	256	
N_{SB} [subcarriers]	19	
Deployment	Small Cell	Large Cell
N_{data}	12	12
L_{filter}	9	8
L_{ZP}	8	7
T_{GP} [μs]	27.34	46.92 (between UL and DL control symbols), 43.01 (otherwise)
Samples in T_{GP}	7	13 (between UL and DL control symbols), 11 (otherwise)
$T_{subframe}$[ms]	7.52	7.52
Samples in subframe	1925	1925
OH_{total}[%]	20.21	20.21
Data rate [Mb/s]	0.3	0.3
HARQ RTT [ms]	30.08	30.08
User density [users/km^2]	2.12M	212
Devices/MHz/km^2	10.6 M	1060
Users/Cell	66,600	66,600

preambles are reserved for IoT devices and are not shared with other services, since the use of narrow band and small subcarrier spacing is more suitable for this service.

Preamble-based RA can enable high user density scenarios but can soon suffer from high collision probability, leading to

high delay and low energy and spectral efficiency, as devices may have to make multiple RA re-trials, leading to multiple preamble transmissions as well as multiple random access response (RAR) message receptions. To support required user density, first, the minimum required number of preambles per subframe must be determined keeping in mind that more preambles imply lower collision probability. It is determined in [52] that for N available preambles, assuming a uniform number of k new users making an RA attempt at every RA slot, k must satisfy $k < c$ for the system to be stable (i.e. being able to cope with the traffic in a finite time, but with an arbitrarily large number of retransmissions), where:

$$c = \left[\log_2\left(\frac{N}{N-1}\right)\right]^{-1} \cdot \left(1 - \frac{1}{N}\right)^{\left[\log_2\left(\frac{N}{N-1}\right)\right]^{-1}} \quad (17)$$

Fig. 9 is a graphical representation of (17). Given that 64 preambles are available in an RA slot and that 10 preambles are reserved for contention-free RA (e.g. for inter-cell handover), 54 preambles are available for contention-based RA. As shown in Fig. 9, a single RA slot enables an average of 18 new users attempting RA per RA slot, in addition to those that collided and are re-trying. Since we target 480,000 users initiating RA within a 300s time window, an average of 12 new users are expected to initiate RA every 7.52 ms. Therefore, according to Fig. 9, an RA slot containing 54 preambles per subframe is sufficient to support the required user density.

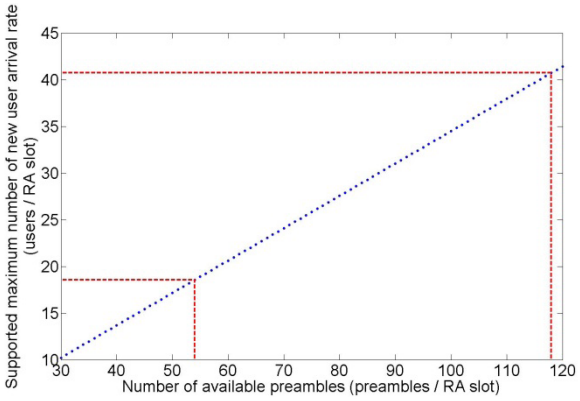

FIGURE 9. Supported new user arrival rate versus number of preambles.

A 4.52 ms RA slot allocated in every 7.52 ms subframe results in less than 3 ms resource for RAR. This 3 ms resource allows for only 20 RARs, assuming an RAR is made up of 56 bits like in LTE [53] and uses uncoded QPSK modulation. Hence, this is not sufficient to respond to every RA attempt. Thus, the use of a second 200 kHz fragment is necessary. The proposed design is presented in Fig. 10. It must be noted that our aim is to design suitable radio frame numerology which allows to enable massive connection requests in IoT scenario. Hence, design of primary/secondary synchronization signals and Physical Broadcast Channel (PBCH) etc. is out of scope of this paper.

Assuming that IoT devices will be less mobile and that inter-cell handover will be rare, only 5 preambles per RA slot are reserved for contention-free RA in this design, i.e. 5 in RA1 and 5 in RA2. A user will randomly pick one of the two slots to transmit one out of the 59 available preambles in the slot. Therefore, there are total 118 RA opportunities every 15.04 ms. As highlighted in Fig. 9, this results in a supported arrival rate of 40 new users per radio frame, for an expected traffic of 24 new users every 15.04 ms. Furthermore, there is sufficient resource for up to 135 56 bits RARs. Note that the number of reserved preambles can be modified in this design and is indicated by the Format Indicator (FI) in Fig. 10.

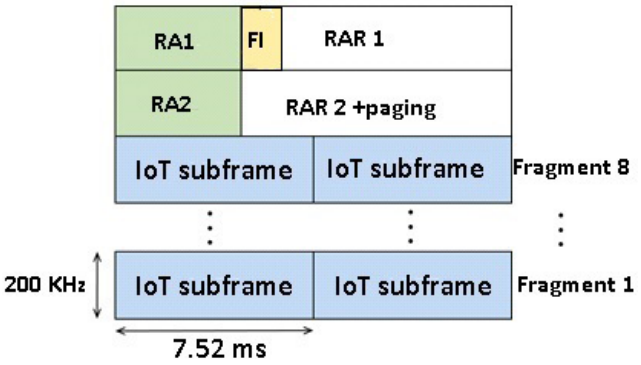

FIGURE 10. Proposed RACH frame design.

Simulations using a Poisson arrival process of mean 24 for new users who randomly pick a preamble among the 118 available showed that the collision probability is $p_{Collision} = 0.222$, leading to 99% of RA success within the first three attempts, given that devices make a new RA attempt immediately after detecting failure (no backoff), and perfect preamble detection conditions at the eNB. This can be further improved by increasing the number of available preambles, provided that there is enough resource for RAR, which will be the topic of future research.

Besides considerations for a better RA procedure to support uplink transmissions, we also introduce a format indicator (FI as shown in Fig. 10) and a paging mechanism for downlink transmissions, for completeness. Depending on the downlink load, a varying number of reserved preambles (indicated by the format indicator) would be allocated to registered devices. These devices have previously established a connection with the cell and possess a unique cell identifier. The cell transmits a paging message with the device's identifier and a reserved preamble. If the device was awake and listening, it will then send its assigned preamble in the next radio frame so as to indicate that it has received the paging message and is now ready to initiate downlink transmission.

IV. SIMULATION RESULTS

The radio frame structure for IoT in 5G has been designed in Section III based on the theoretical analysis to meet the communication requirements in terms of user density and overhead/efficiency. In this section, we will first verify

the selection of proposed key parameters shown in Table 6 and corresponding frame structure in terms of Bit Error Rate (BER) performance via link level simulations. Results of system level simulations will also be presented to assess the system performance and user density in realistic conditions.

A. LINK LEVEL SIMULATIONS

We use Monte-Carlo simulations to examine the system performance in the presence of the transceiver imperfections such as CFO, TO, and Phase Noise (PN). Additionally, in order to investigate the inter-band-interference between frequency chunks for RACH and data transmission in our system, the performance in terms of the minimum output SINR among subcarriers in two chunks is evaluated to provide useful guidance for guard band selection. Results are compared with the OFDM system and simulations are performed in ITU Urban Micro (UMi) channel model. The signal is modulated using QPSK with code rate of 1/2. We use Finite Impulse Response (FIR) Chebyshev filter [3], [43] with 50 dB side lobe attenuation for sub-band filtering. Other simulation parameters for frame structure are listed in Table 6, unless specified otherwise. Note that for all the simulations, low-complexity maximum Log Likelihood Ratio (LLR) based algorithm is used assuming the interference-plus-noise has Gaussian distribution [54]. For fair comparison, the CP length for OFDM system is the same as the filter tail length for UFMC system.

Fig. 11 examines the impact of CFO on the system performance in terms of coded BER. Note that the residual CFO, normalized by subcarrier spacing, i.e. ε for LTE system is assumed in the order of 10^{-3}. For IoT devices, constrained by algorithm/device complexity and cost, we assume the normalized residual CFO varying from $\varepsilon = [0, 0.02, 0.04, 0.06, 0.08, 0.1]$. With the subcarrier spacing Δf=2 kHz, corresponding absolute residual CFO values are $\bar{\varepsilon} = [0, 40, 80, 120, 160, 200]$ Hz, respectively. As we can see from Fig. 11, the performance is not significantly affected by the CFO even with relatively large error. The impact of synchronization error on BER is shown in Fig. 12 by varying the normalized (by the symbol duration) residual TO from $\tau = [0, 0.02, 0.04, 0.06, 0.1]$. For subcarrier spacing Δf =2 kHz and symbol duration T_u = 0.5 ms, the corresponding TO is $\bar{\tau}$ = [0, 0.01, 0.02, 0.03, 0.05] ms. Fig. 12 shows that the system performance degrades significantly when $\tau > 0.06$.

Different from the performance loss caused by CFO and TO, whose values are affected by subcarrier spacing (or symbol duration), the PN caused performance loss, however, is affected by the sampling interval of the system T_s (i.e., 3.9063 us). Here, we assume the phase noise follows the Wiener processing as $\theta_{n+1} = \theta_n + \varphi_n$ with φ_n being a zero-mean Gaussian distributed random variable with variance $\beta = 4\pi\gamma T_s$, where γ is the 3-dB one-side bandwidth of the PN [55]. Intuitively, reducing the sampling rate (i.e., increasing the sample duration) makes the system suffer from significant interference induced by PN. In addition,

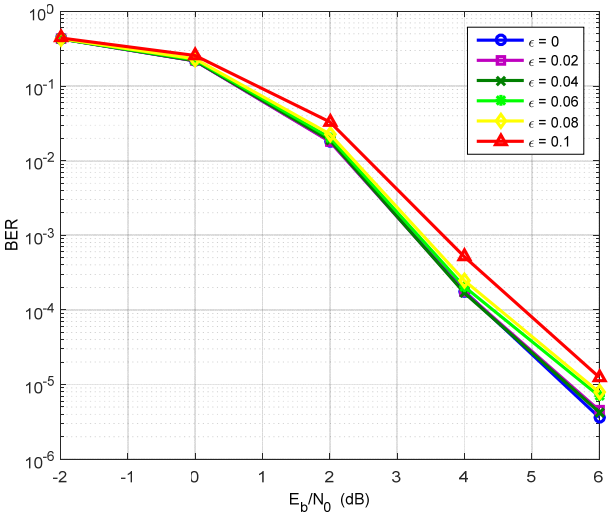

FIGURE 11. BER versus E_b/N_0 for different normalized (by subcarrier spacing) residual CFO (ε).

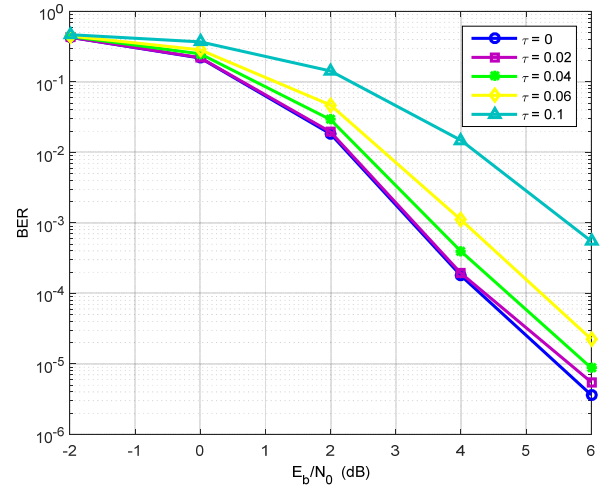

FIGURE 12. BER versus E_b/N_0 for different normalized (by symbol duration) residual TO (τ).

the 3-dB one-side bandwidth of the PN γ depends on the receiver hardware quality and, here, we assume it varies from $\gamma = [0, 10, 20, 50, 100]$ Hz, and the corresponding variance is $\beta = [0, 4, 8, 20, 40]\times 10^{-4}$. We can see from Fig. 13 that the BER performance does not degrade significantly with small γ (e.g., $\gamma < 20$ Hz). However, the degradation is considerable when $\gamma > 20$ Hz with the given proposed system parameters.

In order to investigate the system performance in practice, Fig. 14 shows the simulation results in the presence of all of the aforementioned transceiver imperfections and errors with fixed γ = 20 Hz, $\bar{\varepsilon}$ = 80 Hz, $\bar{\tau}$ = 20 us. Note that for these IoT device and synchronization errors, mitigating the TO by increasing the symbol duration (e.g., reducing subcarrier spacing) may lead to further performance loss from the CFO. Therefore, to achieve a trade-off and optimize the performance, we compare the performance of the system for three different values of subcarrier spacing,

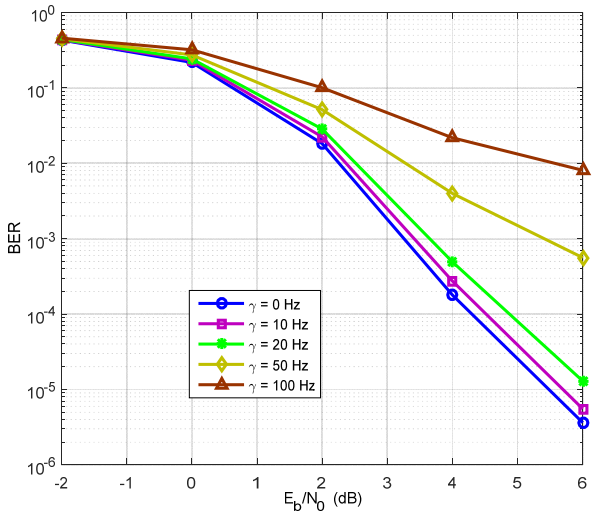

FIGURE 13. BER versus E_b/N_0 as a function of phase noise γ.

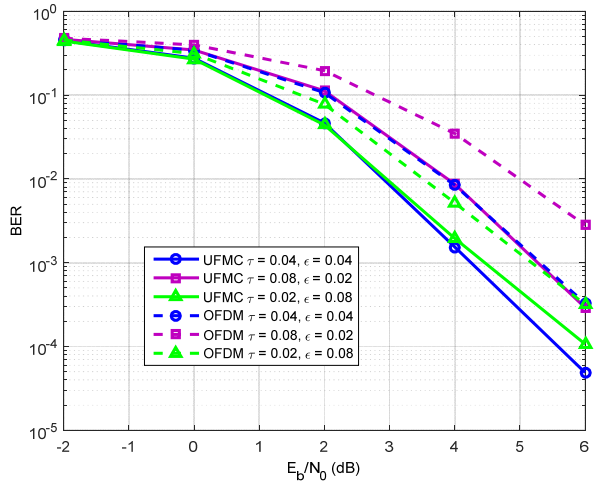

FIGURE 14. BER versus E_b/N_0 for different normalized residual CFO (ε) and normalized residual TO (τ).

i.e. 1 kHz, 2 kHz, and 3 kHz with corresponding normalized CFO and TO as $\varepsilon = [0.008, 0.004, 0.002]$, $\tau = [0.002, 0.004, 0.008]$, respectively. Moreover, performance of OFDM system is also simulated for comparison. From Fig. 14, we can see that the UFMC system can improve the system performance compared with the OFDM system due to the sub-band filtering operation. Moreover, the 2 kHz subcarrier spacing shows the best BER performance in the presence of given errors and imperfections.

Note that the subcarrier spacing in the RA preamble (231 Hz) and data transmission (2 kHz) is different. In principle, combining multiple frames, with different subcarrier spacing for different services, in adjacent frequency bands will destroy the orthogonality of a multi-carrier system resulting in inter- band-interference. In general, a GB is required between services to mitigate the interference. The interference level depends on the subcarrier spacing difference and the GB between the service bands. Moreover, the choice of waveform is also a key factor to determine the interference level. In order to show the impact of GB on the interference between the chunks for RACH and data transmission, we consider two adjacent chunks with chunk 1 used for RACH (with subcarrier spacing 231 Hz) and chunk 2 used for IoT data transmission (with subcarrier spacing 2 kHz). Note that each subcarrier in both chunks suffers from different level of interference. The subcarrier close to the edge of a chunk may suffer from more interference than the one in the middle. We performed simulations to show the worst case of inter-band-interference in terms of the output SINR (with noise power equal to -50 dB to make the system interference limited) among the subcarriers for both chunks by varying the GB. The results for both UFMC and OFDM systems are shown in Fig. 15.

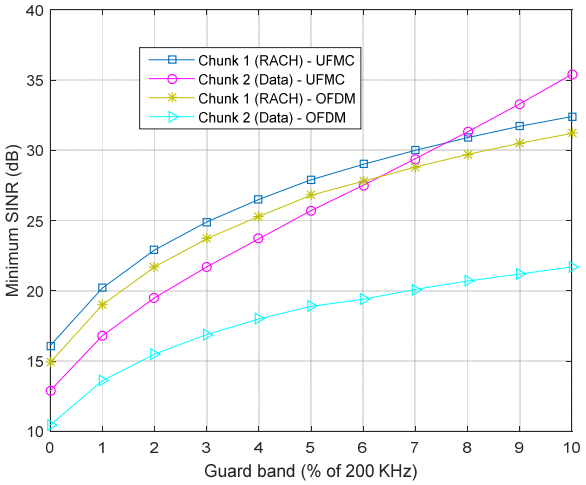

FIGURE 15. Minimum SINR versus guard band for two adjacent frequency chunks carrying RACH and data.

It can be observed from simulation results given in Fig. 15 that when GB increases, minimum SINR also increases. The simulation results also show that 5% of the bandwidth as GB is sufficient to effectively cope with inter-band-interference since the minimum SINR is larger than 25 dB for both chunks. Fig. 15 also shows that with sub-band filtering, the UFMC system can outperform OFDM system in terms of the worst case SINR in all cases.

B. SYSTEM LEVEL SIMULATIONS

Based on numerical value of user density given in Table 6 in Section III.B, it is observed that the proposed design can support upto 66,600 users in 200 kHz bandwidth using uncoded QPSK modulation. Now we present the system level simulation results in order to assess the system performance and capacity under realistic conditions i.e. realistic cell deployments and inter-cell interference conditions.

The considered traffic model follows the parameters of Table 3 while the frame structure and resource grid follow the parameters of Table 6. Additional simulation parameters

TABLE 7. System level simulation parameters.

Parameter	Value
Network topology	7 Macro base stations each with 3 sectors (i.e., 21 cells in total),, wraparound
Inter-site distance	500 m
Scheduler	Round robin
Waveform	UFMC
Link adaptation	CQI-1 to CQI-9
Channel model	ITU-R UMa NLoS [51]
Base station Tx power	46 dBm
Simulation time	300 s, i.e., 39893 TTI
Frequency	1 GHz
Transmission mode	SISO (single-input-single-output)

are provided in Table 7. A single chunk of 200 kHz bandwidth is considered. Link adaptation in terms of modulation/coding is based on channel quality indicator (CQI) feedback adopted from the LTE. The latter defines 15 CQIs with {modulation, code rate} pairs ranging from {QPSK, 0.076} for CQI-1 to {64QAM, 0.93} for CQI-15. However, the rate requirement for IoT users is low as discussed in Section III.A. Thus we consider CQI-9 {16QAM, 0.6} as the maximum modulation/coding that the IoT user can operate with. In order to assess the system performance under several load scenarios as well as to evaluate the peak capacity, several IoT user densities are considered ranging from 6,600 users/cell to 66,000 users/cell with a step of 6,600.

Fig. 16 shows resource usage statistics, i.e., the percentage of the used resource blocks with respect to the total number of resource blocks available during the observation window. The Cumulative Distribution Function (CDF) of the IoT user throughput is provided in Fig. 17 while Fig. 18 shows the average cell (i.e., sector) throughput and spectral efficiency.

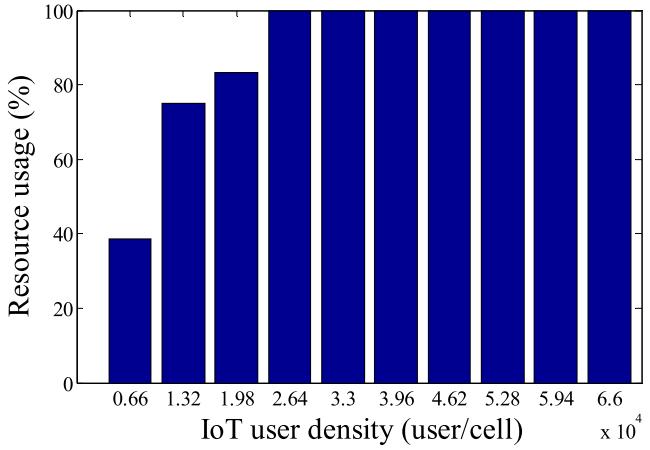

FIGURE 16. Resource usage for underloaded and overloaded scenarios.

As it can be seen in Fig. 16, increasing the IoT user density increases the resource usage until it reaches saturation with density ≥26,400 users/cell. When the system is under loaded (i.e., resource usage <100%), the average cell throughput and

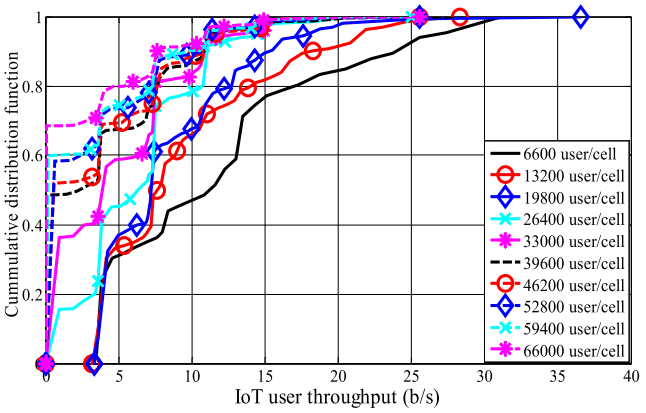

FIGURE 17. CDF of IoT user throughput for underloaded and overloaded scenarios.

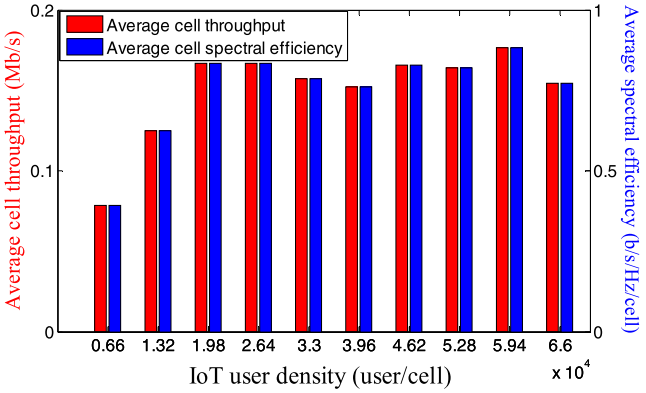

FIGURE 18. Average cell throughput and spectral efficiency for underloaded and overloaded scenarios.

spectral efficiency are proportional to the IoT user density and they reach a peak of 0.17 Mb/s and 0.84 b/s/Hz/cell, respectively, with density = 19, 800 users/cell as shown in Fig. 18. This can be linked to the fact that system throughput (and, hence, spectral efficiency) increases with the user density as long as there are available resources to serve the users. When the resource usage reaches saturation (i.e., user density ≥26,400), then the average cell throughput and spectral efficiency do not increase further and they fluctuate around the peak values.

We consider two metrics: satisfied IoT users and average IoT user throughput, in order to determine the maximum user density that can be supported by the proposed frame structure in a 200 kHz bandwidth. An IoT user is considered to be satisfied if it gets a data rate that can serve all of its traffic, e.g., for a packet size of 125 bytes, a user with a single and two packets in the observation window (i.e. 300 s) is considered to be satisfied if it achieves a data rate of 3.33 b/s and 6.67 b/s respectively. In other words, if all of the packets generated for a single user have been scheduled and successfully received, then this user is considered to be satisfied.

Table 8 provides aggregated results for the two metrics: (1) all IoT users are satisfied, (2) the average IoT user throughput is 3.3 b/s, while Fig. 19 shows CDF of the IoT

TABLE 8. Aggregated simulation results for the user satisfaction and the average rate metrics.

	All IoT users are satisfied	Average IoT user throughput = 3.3 b/s
Maximum density (users/cell)	20,300	46,200
Average cell throughput (Mb/s)	0.16	0.165
Spectral efficiency (b/s/Hz/cell)	0.8	0.83
Resource usage (%)	98.24	100

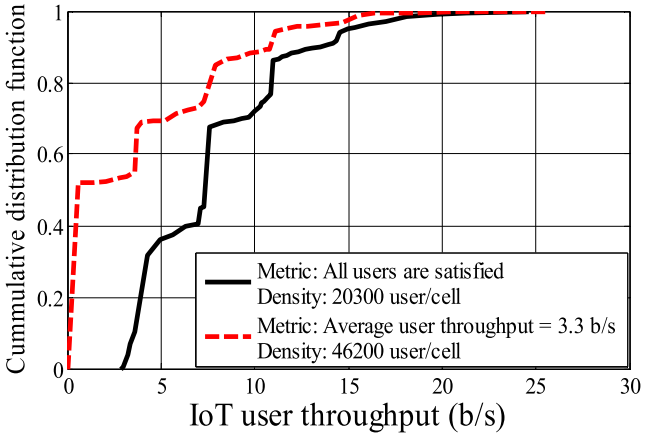

FIGURE 19. CDF of the IoT user throughput for the user satisfaction and the average rate metrics.

user throughput, with 200 kHz bandwidth and frequency reuse of 1. It is observed from results given in Table 8 that, using 200 kHz bandwidth, the proposed IoT frame design can achieve density of 20,300 users/cell for the all users are satisfied metric and 46,200 users/cell for the 3.3 b/s average user throughput metric. These values are, respectively, 69.5% and 30.6% lower than the maximum theoretical value of 66,600 users/cell. It is worth mentioning that obtained density for the 3.3 b/s average user throughput metric (i.e., 46,200 users/cell/200kHz $=$ 231,000 users/cell/MHz) is roughly the same as the density achieved in [46] with the considered metric.

Based on the results of Table 8 and Fig. 19, it can be concluded that the proposed IoT frame structure can reach the 5G target of 480,000 IoT users per cell by using a bandwidth of 4.7 MHz (i.e., 24 chunks of 200 kHz each) whilst ensuring that all IoT users are satisfied. For the 3.3 b/s average user throughput metric, only 2.1 MHz bandwidth (i.e. 11 chunks of 200 kHz bandwidth each) is needed to meet the 5G IoT user density target.

V. CONCLUSION

In this paper, we have discussed the interdependence of different frame design parameters, service requirements and characteristics of radio environment. Based on this interdependency, we have provided guidelines for radio numerology design and elaborated on the frame design for IoT communications in 5G networks to support massive connection density of low-rate, low-power devices. We have also provided simulation results which verify the effectiveness of the proposed numerology in the presence of different transceiver imperfections and also show that the proposed UFMC based design improves the performance as compared to an OFDM system. We also showed via link level simulation results that the selected GB is sufficient to avoid performance degradation due to inter band interference generated due to difference between subcarrier spacing in RACH and data channel. Furthermore, we implemented the proposed IoT frame structure in a system level simulator and provide simulation results to assess the system performance in realistic cell deployments and inter-cell interference conditions. The guidelines provided in this paper, will be used to design frame for other 5G communication scenarios to define a unified frame structure for Multi-Service (MS) 5G networks in future.

APPENDIX

RA in LTE/LTE-A is a preamble-based procedure where UEs randomly choose a preamble from a set of 64 orthogonal preambles, 10 of which are reserved for contention-free RA [19], to transmit in predefined radio resources, namely the physical random access channel (PRACH). It is mainly used to measure timing misalignment due to propagation delay since time synchronisation is necessary for uplink transmission. Therefore, RA occurs in LTE/LTE-A for:

- First connection to the cell (contention-based or contention-free in the case of inter-cell handover)
- Radio link failure to re-establish connection (contention-based)
- Out of synchronisation users that are given a reserved preamble to determine a new timing advance (TA) (contention-free)
- Geolocation for location based services using time difference of arrival (TDOA) of a reserved preamble between different eNodeBs (contention-free)
- Scheduling request (SR) when a RRC_Connected UE was not granted SR resource on the PUCCH (contention-based)

Contention-based RA is a four-step procedure (see Fig. 20) with the following steps [51]:

- Step 1: the UE chooses a random preamble from the 54 orthogonal preambles and transmits it on the PRACH
- Step 2: the eNB sends an RAR on the Physical Downlink Shared Channel (PDSCH) that includes a TA command, a temporary Cell Radio Network Temporary Identifier (C-RNTI) and an uplink grant on the Physical Uplink Shared Channel (PUSCH)
- Step 3: the UE transmits its identity using the C-RNTI to initiate RRC connection
- Step 4: if there was no collision in step 1, the eNB transmits a contention resolution message acknowledging the UE. Otherwise, UEs that collided attempt RA again

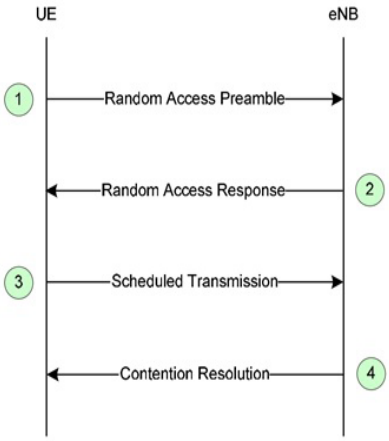

FIGURE 20. **RA procedure in LTE.**

Once RRC connection is established, UEs will then be granted resources to send SR in the PUCCH for uplink transmission.

Collisions can happen at step 1 when two users or more transmit the same preamble. Although possible in some cases [56], it is assumed in LTE/LTE-A that the eNB cannot detect collisions and can only detect that a specific preamble was transmitted. Thus, users that collided at step 1 will go through step 2 and 3 and contention resolution cannot take place before step 4, resulting in additional delay and energy consumption for the UEs that collided.

Note that steps 3 and 4 are not used in contention-free RA. Instead, it consists of three steps as the eNB assigns a preamble before step 1.

ACKNOWLEDGEMENT

The views expressed here are those of the authors and do not necessarily reflect those of the affiliated organisations. The authors would like to acknowledge the support of the University of Surrey 5GIC (http://www.surrey.ac.uk/5gic) members for this work.

REFERENCES

[1] F. Schaich *et al.*, "FANTASTIC-5G: 5G-PPP project on 5G air interface below 6 GHz," in *Proc. Eur. Conf. Netw. Commun.*, Jun. 2015, accessed on Jun. 27, 2016. [Online]. Available: http://fantastic5g.eu/wp-content/uploads/2015/07/EuCNC-FANTASTIC-5G_final.pdf

[2] A. Osseiran *et al.*, "Scenarios for 5G mobile and wireless communications: The vision of the METIS project," *IEEE Commun. Mag.*, vol. 52, no. 5, pp. 26–35, May 2014.

[3] *5G Waveform Candidate Selection*, document 5GNOW_D3.2_v1.3, 5GNOW deliverable D3.2, 2014.

[4] *NGMN 5G White Paper V1.0*, accessed on Apr. 12, 2016. [Online]. Available: https://www.ngmn.org/uploads/media/NGMN_5G_White_Paper_V1_0.pdf

[5] M. Bellanger, "Physical layer for future broadband radio systems," in *Proc. IEEE Radio Wireless Symp. (RWS)*, Jan. 2010, pp. 436–439.

[6] *New SID Proposal: Study on New Radio Access Technology*, document RP-160671, 3GPP TSG RAN Meeting #71, Mar. 2016.

[7] E. Lähetkangas, K. Pajukoski, E. Tiirola, G. Berardinelli, I. Harjula, and J. Vihriälä, "On the TDD subframe structure for beyond 4G radio access network," in *Proc. Future Netw. Mobile Summit (FutureNetworkSummit)*, Lisbon, Portugal, 2013, pp. 1–10.

[8] A. Ijaz, L. Zhang, A. Quddus, and R. Tafazolli, "HARQ in relay-assisted transmission for machine type communications," *IEEE Wireless Commun. Lett.*, vol. 5, no. 2, pp. 172–175, Apr. 2016.

[9] E. Lähetkangas, K. Pajukoski, J. Vihriälä, and E. Tiirola, "On the flexible 5G dense deployment air interface for mobile broadband," in *Proc. 1st Int. Conf. 5G Ubiquitous Connectivity (5GU)*, Akaslompolo, Finland, 2014, pp. 57–61.

[10] T. A. Levanen, J. Pirskanen, T. Koskela, J. Talvitie, and M. Valkama, "Radio interface evolution towards 5G and enhanced local area communications," *IEEE Access*, vol. 2, pp. 1005–1029, 2014.

[11] P. Kela *et al.*, "A novel radio frame structure for 5G dense outdoor radio access networks," in *Proc. IEEE 81st Veh. Technol. Conf. (VTC Spring)*, Glasgow, May 2015, pp. 1–6.

[12] G. Berardinelli, K. Pedersen, F. Frederiksen, and P. Mogensen, "On the design of a radio numerology for 5G wide area," in *Proc. 11th Int. Conf. Wireless Mobile Commun. (ICWMC)*, 2015, pp. 13–18.

[13] K. I. Pedersen, G. Berardinelli, F. Frederiksen, P. Mogensen, and A. Szufarska, "A flexible 5G frame structure design for frequency-division duplex cases," *IEEE Commun. Mag.*, vol. 54, no. 3, pp. 53–59, Mar. 2016.

[14] *The Tactile Internet*, ITU-T Technol. Watch, Aug. 2014. [Online]. Available: https://www.itu.int/dms_pub/itu-t/oth/23/01/T23010000230001PDFE.pdf

[15] M. Agiwal, A. Roy, and N. Saxena, "Next generation 5G wireless networks: A comprehensive survey," *IEEE Commun. Surveys Tuts.*, vol. PP, no. 99, pp. 1–1, doi: 10.1109/COMST.2016.2532458

[16] IMT-2020. (May 2015). *5G Wireless Technology Architecture*, accessed on Apr. 17, 2016. [Online]. Available: http://www.imt-2020.cn/en

[17] Y. Qi, A. U. Quddus, M. AliImran, and R. Tafazolli, "Semi-persistent RRC protocol for machine-type communication devices in LTE networks," *IEEE Access*, vol. 3, pp. 864–874, 2015.

[18] *3rd Generation Partnership Project; Technical Specification Group GSM/EDGE Radio Access Network; Cellular System Support for Ultra-Low Complexity and Low Throughput Internet of Things (CIoT)*, document 3GPP TR 45.820, V13.0.0, 2015.

[19] *3rd Generation Partnership Project; Technical Specification Group Radio Access Network; Study on RAN Improvements for Machine-Type Communications; (Release 11)*, document 3GPP TR 37.868 V11.0.0, 2011.

[20] A. Laya, L. Alonso, and J. Alonso-Zarate, "Is the random access channel of LTE and LTE-A suitable for M2M communications? A survey of alternatives," *IEEE Commun. Surveys Tuts.*, vol. 16, no. 1, pp. 4–16, 1st Quart., 2014.

[21] A. Lo, "Enhanced LTE-advanced random-access mechanism for massive machine-to-machine (M2M) communications," in *Proc. 27th World Wireless Res. Forum Meeting (WWRF)*, 2011, pp. 1–7.

[22] *Evolved Universal Terrestrial Radio Access (E-UTRA); Radio Resource Control (RRC)*, document 3GPP TS 36.331 V10.5.0, Mar. 2012.

[23] *MTC Simulation Results With Specific Solutions*, document R2-104662, 3GPP TSG RAN WG2 #71, ZTE, 2010.

[24] S. Zhang, X. Xu, Y. Wu, L. Lu, and Y. Chen, "A survey on 5G new waveform: From energy efficiency aspects," in *Proc. 48th Asilomar Conf. Signals, Syst. Comput.*, Pacific Grove, CA, USA, 2014, pp. 1939–1943.

[25] F. Schaich and T. Wild, "Waveform contenders for 5G—OFDM vs. FBMC vs. UFMC," in *Proc. 6th Int. Symp. Commun., Control Signal Process. (ISCCSP)*, Athens, Greece, 2014, pp. 457–460.

[26] F. Schaich, T. Wild, and Y. Chen, "Waveform contenders for 5G—Suitability for short packet and low latency transmissions," in *Proc. IEEE 79th Veh. Technol. Conf. (VTC Spring)*, Seoul, South Korea, May 2014, pp. 1–5.

[27] J. Vihriala, N. Ermolova, E. Lahetkangas, O. Tirkkonen, and K. Pajukoski, "On the waveforms for 5G mobile broadband communications," in *Proc. IEEE 81st Veh. Technol. Conf. (VTC Spring)*, Glasgow, Scotland, May 2015, pp. 1–5.

[28] G. Wunder *et al.*, "5GNOW: Non-orthogonal, asynchronous waveforms for future mobile applications," *IEEE Commun. Mag.*, vol. 52, no. 2, pp. 97–105, Feb. 2014.

[29] Y. Chen, F. Schaich, and T. Wild, "Multiple access and waveforms for 5G: IDMA and universal filtered multi-carrier," in *Proc. IEEE Veh. Technol. Conf. (VTC Spring)*, May 2014, pp. 1–5.

[30] V. Vakilian, T. Wild, F. Schaich, S. ten Brink, and J.-F. Frigon, "Universal-filtered multi-carrier technique for wireless systems beyond LTE," in *Proc. IEEE Globecom Workshops (GC Wkshps)*, Dec. 2013, pp. 223–228.

[31] L. Zhang, A. Ijaz, P. Xiao, A. Quddus, and R. Tafazolli, "Single-rate and multi-rate multi-service systems for next generation and beyond communications," in *Proc. IEEE Pers., Indoor Mobile Radio Commun. (PIMRC)*, Sep. 2016.

[32] F. Schaich and T. Wild, "Relaxed synchronization support of universal filtered multi-carrier including autonomous timing advance," in *Proc. Int. Symp. Wireless Commun. Syst. (ISWCS)*, 2014, pp. 203–208.
[33] A. Farhang, N. Marchetti, F. Figueiredo, and J. P. Miranda, "Massive MIMO and waveform design for 5th generation wireless communication systems," in *Proc. Int. Conf. 5G Ubiquitous Connectivity (5GU)*, 2014, pp. 70–75.
[34] V. Venkatasubramanian, M. Hesse, P. Marsch, and M. Maternia, "On the performance gain of flexible UL/DL TDD with centralized and decentralized resource allocation in dense 5G deployments," in *Proc. IEEE PIMRC*, Sep. 2014, pp. 1840–1845.
[35] V. Pauli, Y. Li, and E. Seidel. (Sep. 2015). Dynamic TDD for LTE-A and 5G. Nomor Research, accessed on Apr. 15, 2016. [Online]. Available: http://www.nomor.de/uploads/05/c3/05c398323f99edd96c8a63bf3959466d/WhitePaperNomor_LTE-A_5G-eIMTA_2015-09.pdf
[36] E. Lähetkangas *et al.*, "Achieving low latency and energy consumption by 5G TDD mode optimization," in *Proc. IEEE Int. Conf. Commun. Workshop (ICC)*, Jun. 2014, pp. 1–6.
[37] Y. Wang, K. Valkealahati, K. Shu, R. Shankar, and S. Morgera, "Performance evaluation of flexible TDD switching in 3GPP LTE system," in *Proc. IEEE Sarnoff Symp.*, Newark, NJ, USA, May 2012, pp. 1–4.
[38] D. Zhu and M. Lei, "Cluster-based dynamic DL/UL reconfiguration method in centralized RAN TDD with trellis exploration algorithm," in *Proc. IEEE WCNC*, Apr. 2013, pp. 3758–3763.
[39] B. Yu, S. Mukherjee, H. Ishii, and L. Yang, "Dynamic TDD support in the LTE-B enhanced Local area architecture," in *Proc. IEEE Globecom Workshops*, Dec. 2012, pp. 585–591.
[40] S. Morosi, M. Biagini, F. Argenti, E. Del Re, and L. Yessenturayeva, "Frame design for 5G multicarrier modulations," in *Proc. Int. Wireless Commun. Mobile Comput. Conf. (IWCMC)*, Dubrovnik, Croatia, 2015, pp. 1000–1005.
[41] H. Holma and A. Toskala, Eds., *LTE for UMTS: OFDMA and SC-FDMA Based Radio Access*. New York, NY, USA: Wiley, 2009.
[42] J. G. Andrews *et al.*, "What will 5G be?" *IEEE J. Sel. Areas Commun.*, vol. 32, no. 6, pp. 1065–1082, Jun. 2014.
[43] L. Zhang, A. Ijaz, P. Xiao, M. A. Imran, and R. Tafazolli, "MU-UFMC system performance analysis and optimal filter length and zero padding length design," *IEEE Trans. Commun.*, to be published. [Online]. Available: https://www.researchgate.net/publication/301855638_MU-UFMC_System_Performance_Analysis_and_Optimal_Filter_Length_and_Zero_Padding_Length_Design
[44] E. Läehetkangas *et al.*, "On the selection of guard period and cyclic prefix for beyond 4G TDD radio access network," in *Proc. 19th Eur. Wireless Conf. (EW)*, Guildford, U.K., 2013, pp. 1–5.
[45] *Scenarios, Requirements and KPIs for 5G Mobile and Wireless System*, document ICT-317669-METIS/D1.1, METIS deliverable D1.1, Apr. 2013.
[46] R. Ratasuk, J. Tan and, and A. Ghosh, "Coverage and Capacity Analysis for Machine Type Communications in LTE," in *Proc. IEEE Veh. Technol. Conf. (VTC Spring)*, Yokohama, Japan, May 2012, pp. 1–5.
[47] *Simulation Guidelines*, document ICT-317669-METIS/D6.1, METIS deliverable D6.1, Oct. 2013.
[48] 4G Americas White Paper. (Aug. 2015). *5G Spectrum Recommendations*, accessed on Jun. 27, 2016. [Online]. Available: http://www.4gamericas.org/files/6514/3930/9262/4G_Americas_5G_Spectrum_Recommendations_White_Paper.pdf
[49] *METIS Channel Models*, document ICT-317669-METIS/D1.4, METIS Deliverable D1.4, Feb. 2015.
[50] *Guidelines for Evaluation of Radio Interface Technologies for IMT-Advanced*, document ITU-R M.2135-1, 2009.
[51] *3rd Generation Partnership Project; Technical Specification Group Radio Access Network; Evolved Universal Terrestrial Radio Access (E-UTRA) and Evolved Universal Terrestrial Radio Access Network (E-UTRAN); Overall Description; Stage2 (Release 13)*, document 3GPP TS 36.300 V13.3.0, 2016.
[52] L. Tello-Oquendo, I. Leyva-Mayorga, V. Pla, J. Martinez-Bauset, and V. Casares-Giner, "Analysis of LTE-A random access procedure: A foundation to propose mechanisms for managing the M2M massive access in wireless cellular networks?" in *Proc. Workshop Innov. Inf. Commun. Technol.*, 2015, pp. 95–101.
[53] *3rd Generation Partnership Project; Technical Specification Group Radio Access Network; Evolved Universal Terrestrial Radio Access (E-UTRA) Medium Access Control (MAC) Protocol Specification (Release 13)*, document 3GPP TS 36.321 V13.1.0, 2016.
[54] Q. Wang, Q. Xie, Z. Wang, S. Chen, and L. Hanzo, "A universal low-complexity symbol-to-bit soft demapper," *IEEE Trans. Veh. Technol.*, vol. 63, no. 1, pp. 119–130, Jan. 2014.
[55] R. Hamila, O. Özdemir, and N. Al-Dhahir, "Beamforming OFDM performance under joint phase noise and I/Q imbalance," *IEEE Trans. Veh. Technol.*, vol. 65, no. 5, pp. 2978–2989, May 2015.
[56] S. Sesia, I. Toufik, and M. Baker, Eds., *LTE—The UMTS Long Term Evolution: From Theory to Practice*. New York, NY, USA: Wiley, 2009.

AYESHA IJAZ received the B.Eng. degree in electronic engineering from the University of Engineering amnd Technology, Taxila, Pakistan, in 2006, and the M.Sc. and Ph.D. degrees in mobile and satellite communications from the University of Surrey, Guildford, U.K., in 2008 and 2011, respectively. She is currently a Research Fellow with the Institute for Communication Systems, Home of 5G Innovation Centre, University of Surrey, U.K. Her research interests include statistical signal processing and air-interface design for next generation wireless communication systems.

LEI ZHANG received the B.Eng. degree in communication engineering and the M.Sc. degree in electromagnetic fields and microwave technology from Northwestern Polytechnic University, Xi'an, China, in 2005 and 2008, respectively, and the Ph.D. degree from the Communications Research Group, University of Sheffield, U.K., in 2011. He is currently a Research Fellow in Wireless Communications with the Institute of Communications (ICS), University of Surrey, U.K.. Before he joined ICS, he was a Research Engineer with Huawei technologies, China. His research interests include multi-antenna signal processing, air interface waveform design, cloud radio access networks, massive MIMO systems.

MAXIME GRAU received the B.Eng. degrees in electrical engineering and telecommunications engineering from CentraleSupélec, Campus de Gif-Sur-Yvette, France, in 2012 and 2015, respectively, and the M.Sc. degree in advance wireless communications from CentraleSupélecn ENS Cachan and Université Paris-Sud XI, France. He is currently pursuing the Ph.D. degree with the Institute for Communication Systems, University of Surrey, U.K.. He is currently involved in the system architecture and co-existence work area in the 5G Innovation Centre, Surrey. His current research interests include the Internet of Things, random access, and control/data separation.

ABDELRAHIM MOHAMED received the B.Sc. degree (Hons.) in electrical and electronics engineering from the University of Khartoum, Sudan, in 2011, and the M.Sc. degree (Hons.) in mobile and satellite communications from the University of Surrey, U.K., in 2013 where he secured the first place in the Electronics Engineering Department. He is currently pursuing the Ph.D. degree with the Institute for Communication Systems, University of Surrey. He was involved in the FP7 CoRaSat project and currently involved in the System Architecture and Coexistence work area in the 5G Innovation Centre, Surrey. His current research interests include radio access networks with control/data plane separation, energy efficiency, mobility management, and cognitive radio.

SERDAR VURAL received the M.Sc. and Ph.D. degrees in electrical and computer engineering from the Ohio State University, Columbus, OH, USA, in 2005 and 2007, respectively, and the B.S. degree in electrical and electronics engineering from Bo?aziçi University, Istanbul, Turkey in 2003. He is currently a Research Fellow with the 5G Innovation Centre, Institute for Communication Systems, University of Surrey, U.K.. His current research interests include wireless sensor, ad hoc, mesh networks, Internet-of-Things, machine-to-machine communications, future Internet, information-centric networking, and next generation mobile networks.

ATTA U. QUDDUS received the M.Sc. degree in satellite communications and the Ph.D. degree in mobile cellular communications from the University of Surrey, U.K., in 2000 and 2005, respectively. He is currently a Lecturer in Wireless Communications with the Institute of Communications, Department of Electronic Engineering, University of Surrey. During his research career, he has led several national and international research projects that also contributed towards 3GPP standardization. In 2004, he also won the Centre for Communications Systems Research Excellence Prize sponsored by Vodafone for his research on adaptive filtering algorithms. His current research interests include Machine Type Communication, Cloud Radio Access Networks, and Device to Device Communication.

MUHAMMAD ALI IMRAN (SM'12) received the M.Sc. (Hons.) and Ph.D. degrees from Imperial College London, U.K., in 2002 and 2007, respectively. He is currently a Reader (Associate Professor) with the Institute for Communication Systems, University of Surrey, U.K., and an Adjunct Associate Professor with the University of Oklahoma, USA. He had a leading role in a number of multimillion international research projects encompassing the areas of energy efficiency, fundamental performance limits, sensor networks and self-organizing cellular networks. He is also leading the new physical layer work area for 5G innovation centre and the curriculum development for the new Engineering for Health program at Surrey. He has a global collaborative research network spanning both academia and key industrial players in the field of wireless communications. He has supervised more than 20 successful Ph.D. graduates. He has contributed to ten patents and published over 200 peer-reviewed research papers, including more than 20 IEEE Transactions. He has been awarded IEEE Comsocs Fred Ellersick Award 2014, the FEPS Learning and Teaching Award 2014, and twice nominated for the Tony Jeans Inspirational Teaching Award. He was a shortlisted finalist for The Wharton-QS Stars Awards 2014 for innovative teaching and VC's learning and teaching award in the University of Surrey. He has acted as a Guest Editor of *IET Signal Processing*, the *IEEE Communications Magazine*, the *IEEE Wireless Communication Magazine*, and the IEEE Access. He is an Associate Editor of the IEEE Communications Letters, the IEEE Access, and *IET Communications Journal*. He is a Senior Fellow of Higher Education Academy U.K.

CHUAN HENG FOH received the M.Sc. degree from Monash University, Australia, in 1999, and the Ph.D. degree from the University of Melbourne, Australia, in 2002. After his Ph.D., he joined Monash University, Australia, and then Nanyang Technological University, Singapore. He is with University of Surrey, U.K. He is currently an Associate Editor of the IEEE Access, the IEEE Wireless Communications, and the *International Journal of Communications Systems*. He is also the Vice Chair (Europe/Africa) of the IEEE Technical Committee on Green Communications and Computing. His research interests include protocol design and performance analysis of various computer networks, including wireless local area and mesh networks, mobile ad hoc and sensor networks, Internet of Things, 5G networks, and data center networks.

RAHIM TAFAZOLLI is a Professor and the Director of the Institute for Communication Systems (ICS) and 5G Innovation Centre with the University of Surrey, U.K. He has published more than 500 research papers in refereed journals, international conferences and as invited speaker. He is the Editor of two books on *Technologies for Wireless Future* (Wiley, 2004 and 2006). He was appointed as a fellow of the Wireless World Research Forum in 2011, in recognition of his personal contribution to the wireless world. As well as heading one of Europe's leading research groups.